

## **Cationic modified Fe-N-C catalyst for electrochemical reduction of nitrate in solution with low ionic strength**

**AUTHORS:** Lin-Feng Yang, Hai-Gang Qin, Fu-Zhi Li, Jian-Zhao Peng, Jun Gu \*

**AFFILIATION:**

Department of Chemistry, Southern University of Science and Technology, Shenzhen,  
Guangdong 518055, China.

Corresponding author E-mail: [guj6@sustech.edu.cn](mailto:guj6@sustech.edu.cn)

**Chemicals:** Anhydrous iron(II) chloride ( $\text{FeCl}_2$ , 99.5%, Energy Chemical), zinc nitrate hexahydrate ( $\text{Zn}(\text{NO}_3)_2 \cdot 6\text{H}_2\text{O}$ , 99%, Aladdin), 2-methylimidazole (2-mIm, 99.85%, Bidepharm), potassium iodide (KI, 99.2%, Bidepharm), methyl iodide ( $\text{CH}_3\text{I}$ , 98%, Adamas), Poly(4-vinylpyridine) ( $\text{C}_7\text{H}_7\text{N}$ , MW~60000, Macklin), methanol (MeOH, 99.5%, General Reagent), ethanol (EtOH, 99.7%, General Reagent), hydrochloric acid ( $\text{HCl}$ , 36%, Dongjiang Reagent), nitric acid ( $\text{HNO}_3$ , 65%, Yonghuachem), sodium hydroxide ( $\text{NaOH}$ , 96%, Yonghuachem), sodium nitrate ( $\text{NaNO}_3$ , 99.0%, Anpel), salicylic acid ( $\text{C}_7\text{H}_6\text{O}_3$ , 98%, Bidepharm), sodium citrate ( $\text{C}_6\text{H}_5\text{Na}_3\text{O}_7$ , 98%, Adamas), sodium nitroprusside ( $\text{C}_5\text{FeN}_6\text{Na}_2\text{O}$ , AR, Macklin), sulfanilamide ( $\text{C}_6\text{H}_8\text{N}_2\text{O}_2\text{S}$ , 99%, Aladdin), sodium hypochlorite solution ( $\text{NaClO}$ , 0.1M, Macklin), phosphorous acid ( $\text{H}_3\text{PO}_4$ , 85% in water, General Reagent), N-(1-naphthyl) ethylenediamine dihydrochloride ( $\text{C}_{12}\text{H}_{14}\text{N}_2 \cdot 2\text{HCl}$ , 98%, Macklin) and sodium perchlorate monohydrate ( $\text{NaClO}_4 \cdot \text{H}_2\text{O}$ , 99.99%, Aladdin) were used as received without any purification.

**Characterizations:** The X-ray diffraction (XRD) patterns were collected with a Rigaku SmartLab X-ray powder diffractometer using  $\text{Cu K}\alpha$  radiation. The X-ray photoelectron spectrum (XPS) characterizations were performed on an ULVAC-PHI 5000 VersaProbe III XPS system using monochromatic  $\text{Al K}\alpha$  radiation (1486.6 eV). TEM, HAADF-STEM and EDX mapping images were performed on an FEI Talos F200X G2 operated at 200 kV. Atomic resolution HAADF-STEM images were performed on an FEI Titan Themis G2 at 300 kV with spherical aberration corrected. The Ultraviolet-visible (UV-Vis) absorbance data were measured on Agilent Cary 8454 spectrophotometer. The ICP-AES data were obtained on a Thermo iCAP 7000 SERIES instrument. The Fourier transform infrared (FT-IR) spectrum data were recorded on a Bruker Vertex 70v spectrometer. Zeta potentials were measured on a ZetaPALS zeta potential analyzer.

**Synthesis of partially methylated P4VP:** 150 mg of Poly(4-vinylpyridine) (P4VP) was added into 2.0 mL of  $\text{CH}_3\text{I}$  and then stirred in Ar at 50 °C for 2 hours. The product was then separated by a rotary evaporator and dried under vacuum at room temperature for 3 hours.

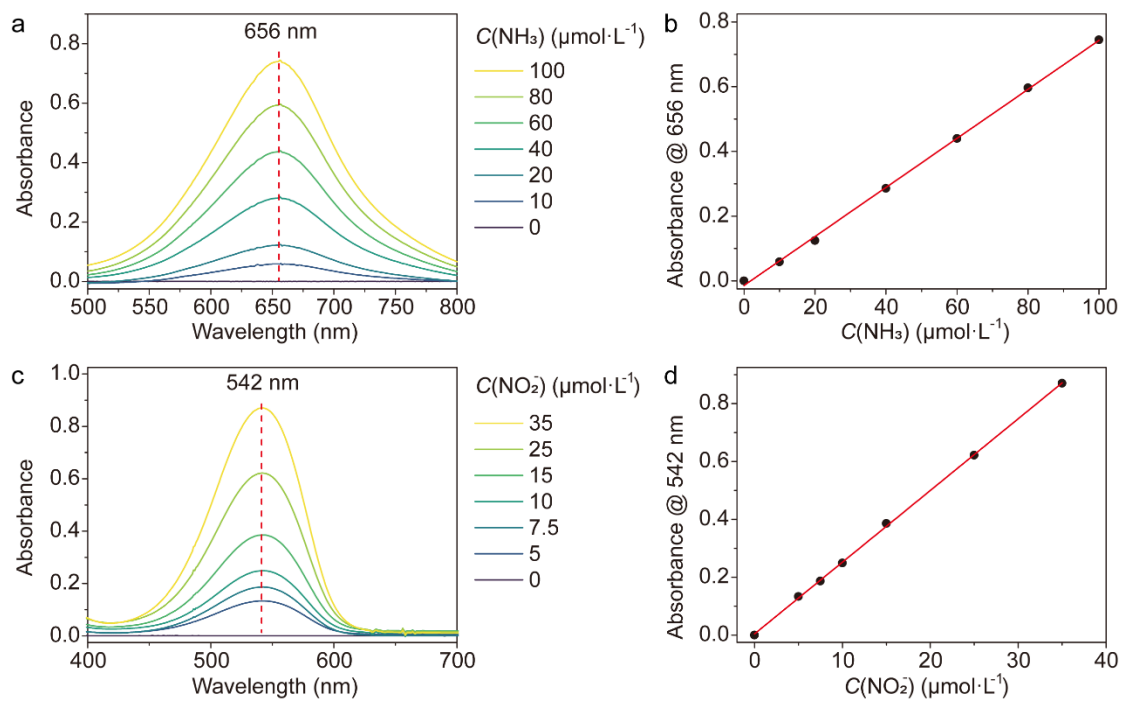


**Figure S1.** Absorption spectra (a, c) and corresponding standard curves (b, d) of  $\text{NH}_4\text{Cl}$  (a, b) and  $\text{NaNO}_2$  (c, d) solutions.

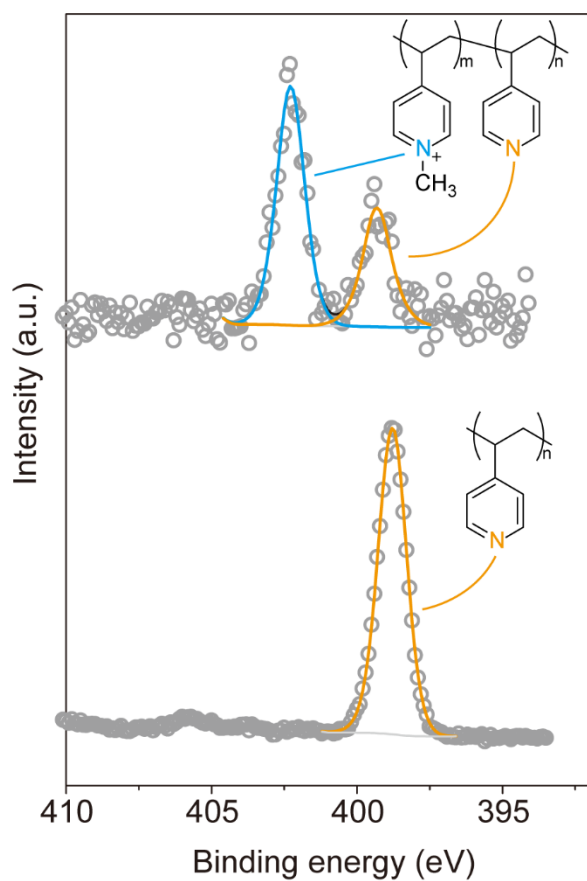


**Figure S2.** N 1s XPS spectra of P4VP (bottom) and partially methylated P4VP (top). The orange and blue peaks were assigned to pyridinic N and cationic N, respectively.

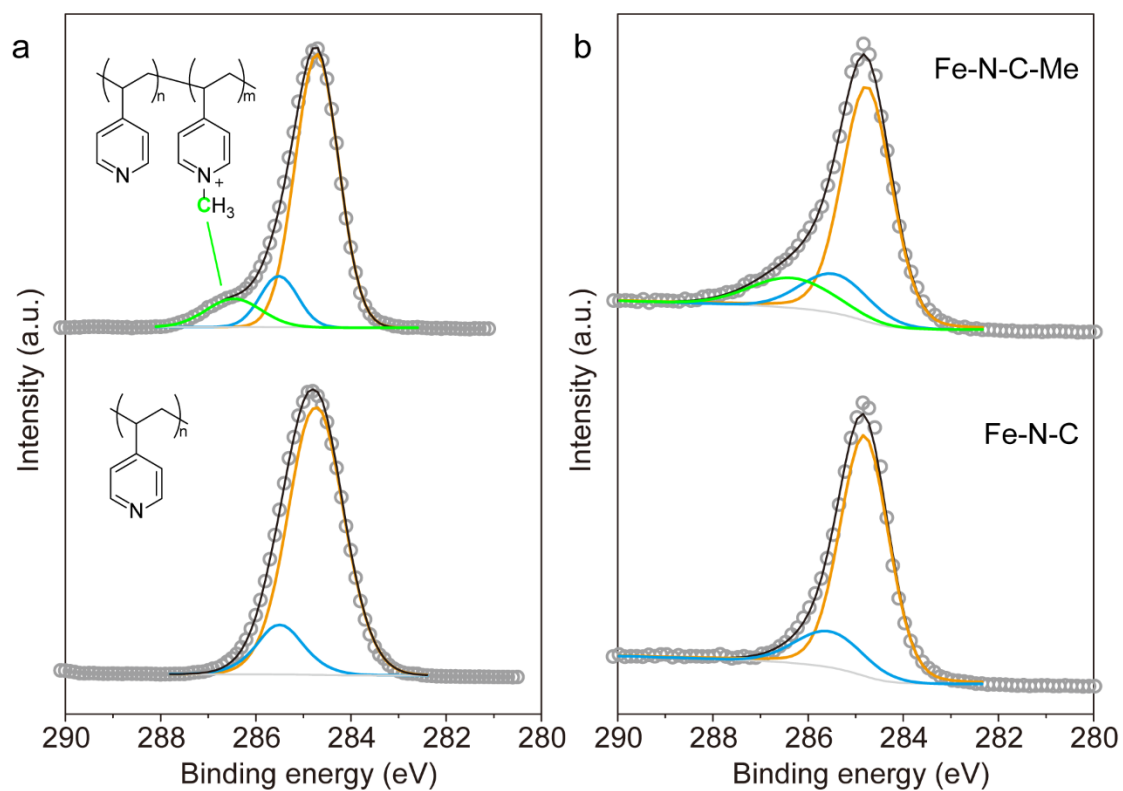


**Figure S3.** Characterization of methyl groups attached to cationic N sites by C 1s XPS spectra. (a) Spectra of P4VP (bottom) and partially methylated P4VP (top). (b) Spectra of Fe-N-C (bottom) and Fe-N-C-Me (top). The orange, blue and green peaks were assigned to C atoms in C-C, C-N and N<sup>+</sup>-CH<sub>3</sub> moieties, respectively.

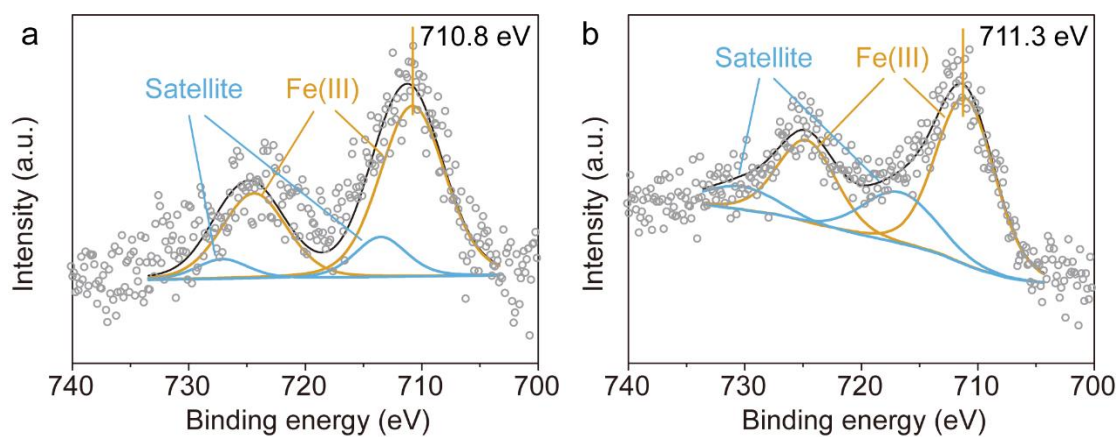


**Figure S4.** Fe 2p XPS spectra of (a) Fe-N-C and (b) Fe-N-C-Me. The spectra were deconvoluted into  $2p^{3/2}$  and  $2p^{1/2}$  peaks of Fe(III) species (orange) and satellite features (blue). Circles show the data and solid curves show the fitting.

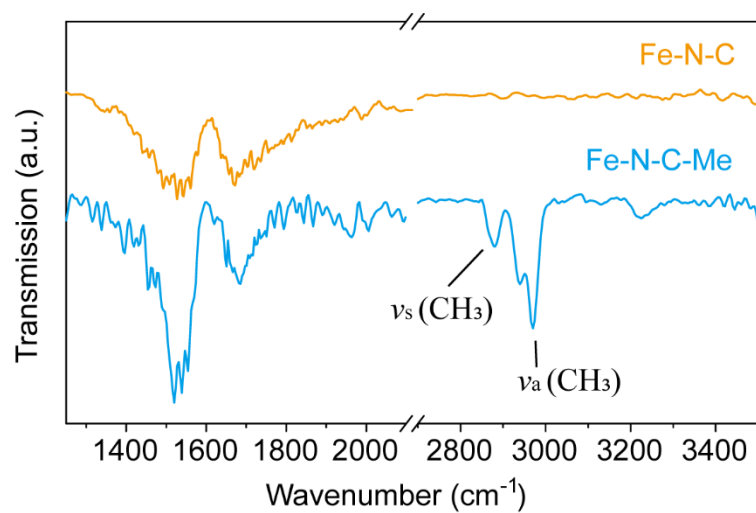


**Figure S5.** IR spectra of Fe-N-C and Fe-N-C-Me.

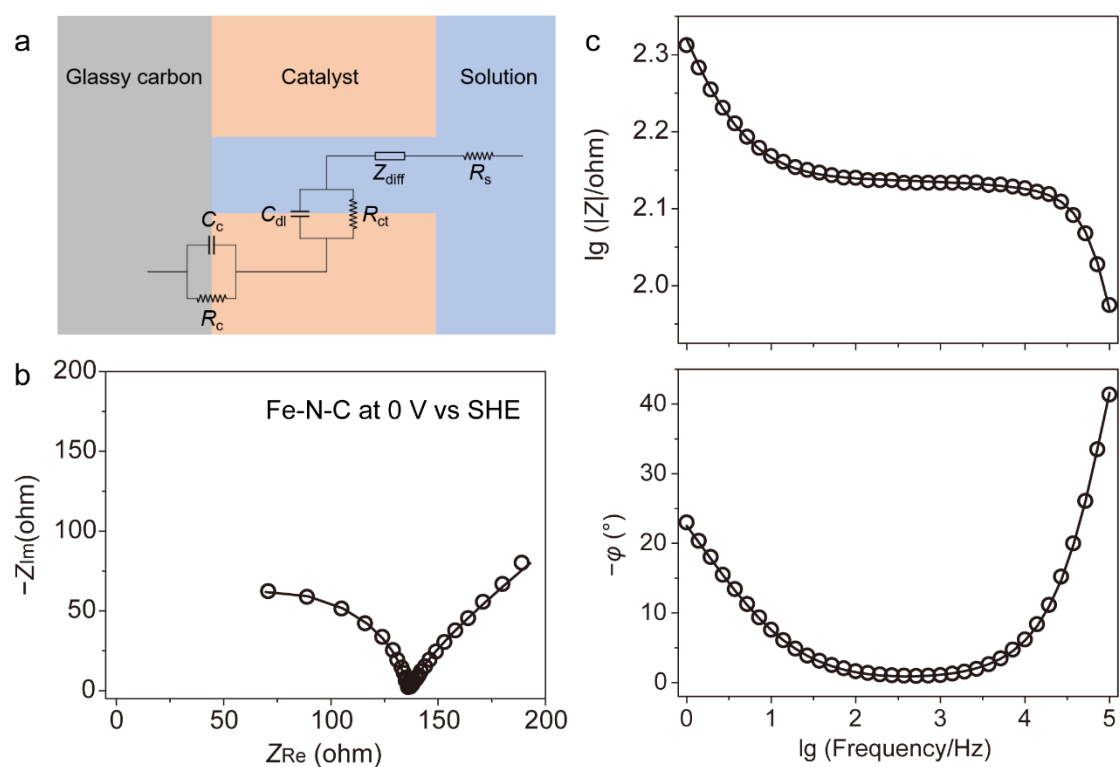


**Figure S6.** Fitting of EIS spectra in solution containing 1 mM of  $\text{NaClO}_4$ . (a) Schematic of equivalent circuit for the fitting.  $C_c$  and  $R_c$  are the contact capacitance and resistance between glassy carbon electrode and the catalyst material, respectively. The resistance of electron movement in the catalyst is neglected due to the high conductivity of the carbon matrix.  $C_{dl}$  is the double layer capacitance between catalyst and solution.  $R_{ct}$  is the resistance of charge transfer at the catalyst-solution interface.  $Z_{diff}$  is the impedance of diffusion of ions.  $R_s$  is the resistance of solution. Example of (b) Nyquist plot and (c) Bode plot used for fitting: Fe-N-C at 0 V vs SHE. Circles are experimental data and lines are fitting curves.

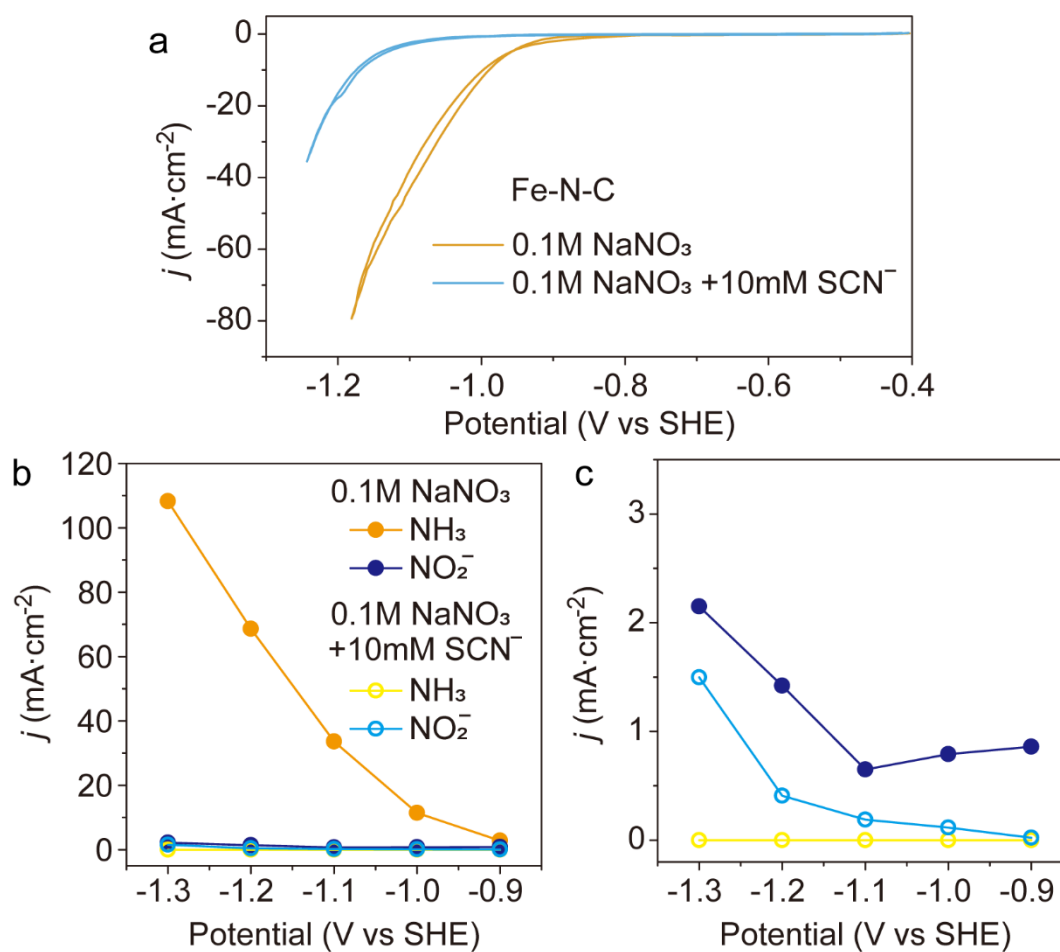


**Figure S7.** Comparison of the electrocatalytic performances of Fe-N-C with and without  $\text{SCN}^-$ . (a) CV curves of Fe-N-C in solution containing 0.1 M of  $\text{NaNO}_3$  (orange) and in solution containing 0.1 M of  $\text{NaNO}_3$  and 10 mM of KSCN (blue). (b) Partial current density of  $\text{NH}_3$  (orange and yellow) and  $\text{NO}_2^-$  (dark and light blue) of Fe-N-C in solution containing 0.1 M of  $\text{NaNO}_3$  (solid circles) and in solution containing 0.1 M of  $\text{NaNO}_3$  and 10 mM of KSCN (hollow circles). (c) Enlargement of panel (b) between 0 and 3  $\text{mA}\cdot\text{cm}^{-2}$ .

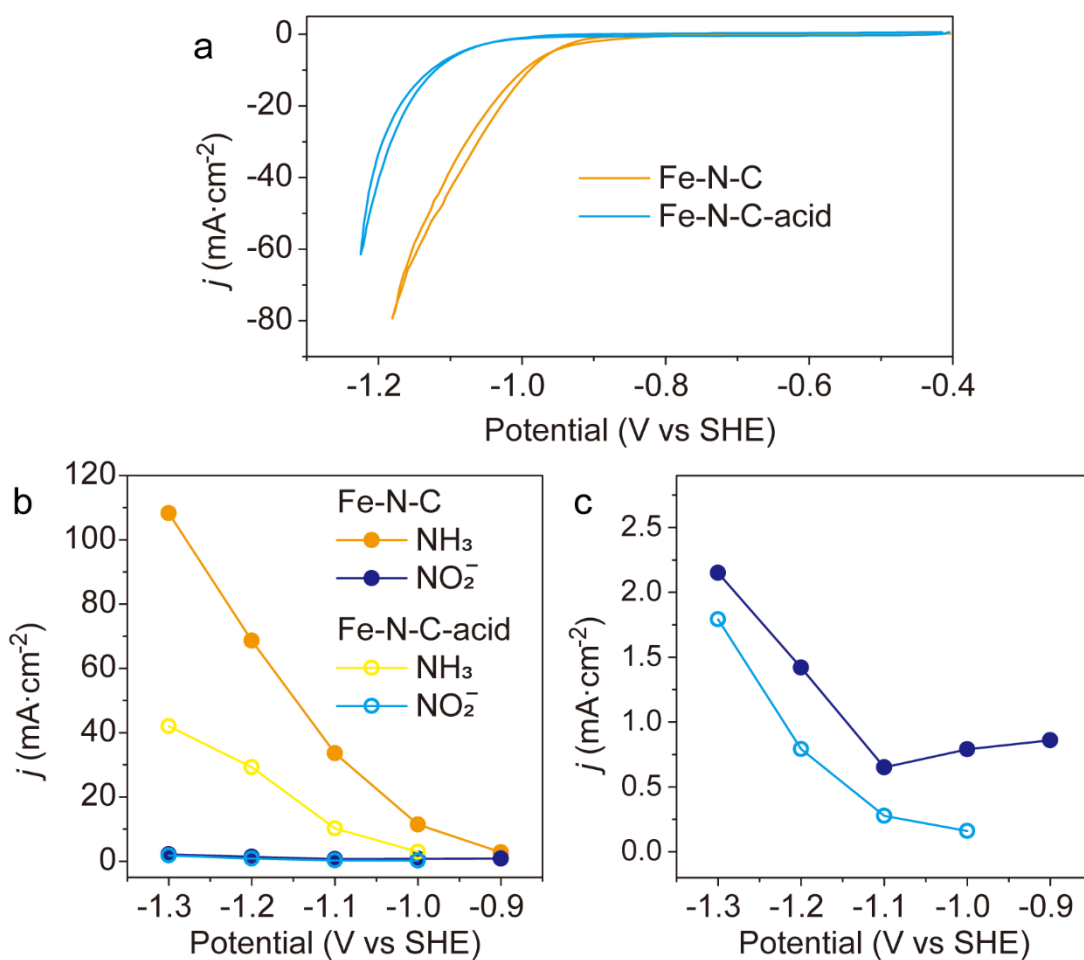
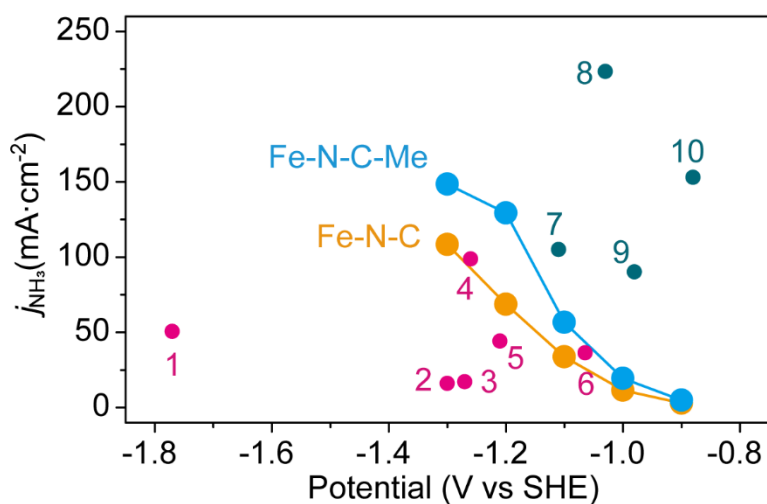


**Figure S8.** Comparison of the electrocatalytic performances of Fe-N-C and Fe-N-C-acid in solution containing 0.1 M of NaNO<sub>3</sub>. (a) CV curves. (b) Partial current density of NH<sub>3</sub> (orange and yellow) and NO<sub>2</sub><sup>-</sup> (dark and light blue) of Fe-N-C (solid circles) and Fe-N-C-acid (hollow circles). (c) Enlargement of panel (b) between 0 and 2.5 mA·cm<sup>-2</sup>.



Reference	Catalyst	Solution	Highest FE of NH <sub>3</sub>
This work	Fe-N-C-Me	0.1 M NaNO <sub>3</sub>	96%
This work	Fe-N-C	0.1 M NaNO <sub>3</sub>	96%
1	Cu-N-C SAC	0.1 M KNO <sub>3</sub> + 0.1 M KOH	85%
2	In-S-G	0.1 M KNO <sub>3</sub> + 1 M KOH	75%
3	Fe-PPy SACs	0.1 M KNO <sub>3</sub> + 0.1 M KOH	100%
4	Fe SAC	0.5 M KNO <sub>3</sub> + 0.1 M K <sub>2</sub> SO <sub>4</sub>	67%
5	Ni <sub>35</sub> /NC-sd	0.3 M NaNO <sub>3</sub> + 0.5 M Na <sub>2</sub> SO <sub>4</sub>	77%
6	CoO <sub>x</sub> nanosheets	0.1 M KNO <sub>3</sub> + 0.1 M KOH	93%
7	Pd(111)	0.1 M NaNO <sub>3</sub> + 0.1 M Na <sub>2</sub> SO <sub>4</sub>	80%
8	Strained Ru nanoclusters	1 M KNO <sub>3</sub> + 1 M KOH	100%
9	Cu <sub>50</sub> Ni <sub>50</sub> alloy	0.1 M KNO <sub>3</sub> + 1 M KOH	99%
10	Rh@Cu-0.6%	0.1 M KNO <sub>3</sub> + 0.1 M Na <sub>2</sub> SO <sub>4</sub>	93%

**Figure S9.** Comparison of partial current density of NH<sub>3</sub> of Fe-N-C (orange), Fe-N-C-Me (blue) and the state-of-the-art catalysts (dark green: metallic Cu and noble metal-based catalysts; pink: other catalysts). The table below lists the references, names, electrolyte composition and highest FE of NH<sub>3</sub> of each catalyst.<sup>1-10</sup>

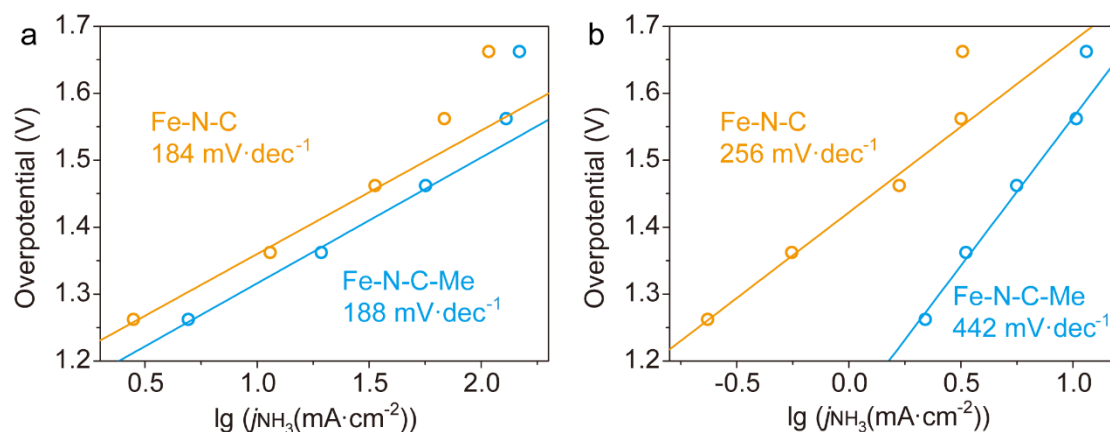


**Figure S10.** Tafel analysis of ammonia formation on Fe-N-C (orange) and Fe-N-C-Me (blue) in (a) 0.1 M of  $\text{NaNO}_3$  and (b) 1 mM of  $\text{NaNO}_3$  and 30 mM of  $\text{NaClO}_4$ . The overpotential was calculated based on the fact that the equilibrium potential for ammonia formation ( $\text{NO}_3^- + 10\text{H}^+ + 8\text{e}^- \rightarrow \text{NH}_4^+ + 3\text{H}_2\text{O}$ ) at pH 7 is 0.36 V vs SHE. However, since the electrolyte was not buffered, the local pH near cathode was significantly higher than 7. A large fraction of overpotential was originated from the nonuniform pH distribution.

**Table S1.** Fitting of high-resolution N 1s XPS spectra of Fe-N-C and Fe-N-C-Me.

		Fe-N-C	Fe-N-C-Me
Pyridinic N	Binding energy (eV)	398.5	398.5
	Percentage (%)	47	29
Fe-N <sub>x</sub>	Binding energy (eV)	400.4	400.4
	Percentage (%)	23	22
Pyrrolic N	Binding energy (eV)	401.4	401.3
	Percentage (%)	30	17
Cationic N	Binding energy (eV)	--	402.2
	Percentage (%)	--	32

**Table S2.** Concentration of ionic species (unit: mM) and ionic strength (unit: mM) of river water in Dezhou, Shandong, China.<sup>11</sup>

	Ca <sup>2+</sup>	Mg <sup>2+</sup>	Na <sup>+</sup>	K <sup>+</sup>	HCO <sub>3</sub> <sup>-</sup>	SO <sub>4</sub> <sup>2-</sup>	Cl <sup>-</sup>	NO <sub>3</sub> <sup>-</sup>	Ionic strength*
Max.	4.07	5.54	27.15	1.42	11.75	8.26	23.47	2.39	68.83
Min.	1.11	1.15	2.77	0.04	0.78	1.14	4.93	0.003	11.06
Mean	2.19	3.78	10.43	0.62	6.41	3.75	10.92	0.80	34.03

\* Ionic strength was calculated according to:

$$I = \frac{1}{2} \sum_i c_i z_i^2$$

In this equation,  $c_i$  and  $z_i$  are the molarity and charge number of species  $i$ , respectively.

## REFERENCES:

1. J. Yang, H. Qi, A. Li, X. Liu, X. Yang, S. Zhang, Q. Zhao, Q. Jiang, Y. Su, L. Zhang, J.-F. Li, Z.-Q. Tian, W. Liu, A. Wang and T. Zhang, Potential-Driven Restructuring of Cu Single Atoms to Nanoparticles for Boosting the Electrochemical Reduction of Nitrate to Ammonia, *J. Am. Chem. Soc.*, 2022, **144**, 12062-12071.
2. F. Lei, W. Xu, J. Yu, K. Li, J. Xie, P. Hao, G. Cui and B. Tang, Electrochemical synthesis of ammonia by nitrate reduction on indium incorporated in sulfur doped graphene, *Chem. Eng. J.*, 2021, **426**, 131317.
3. P. Li, Z. Jin, Z. Fang and G. Yu, A single-site iron catalyst with preoccupied active centers that achieves selective ammonia electrosynthesis from nitrate, *Energy Environ. Sci.*, 2021, **14**, 3522-3531.
4. Z.-Y. Wu, M. Karamad, X. Yong, Q. Huang, D. A. Cullen, P. Zhu, C. Xia, Q. Xiao, M. Shakouri, F.-Y. Chen, J. Y. Kim, Y. Xia, K. Heck, Y. Hu, M. S. Wong, Q. Li, I. Gates, S. Siahrostami and H. Wang, Electrochemical ammonia synthesis via nitrate reduction on Fe single atom catalyst, *Nat. Commun.*, 2021, **12**, 2870.
5. P. Gao, Z.-H. Xue, S.-N. Zhang, D. Xu, G.-Y. Zhai, Q.-Y. Li, J.-S. Chen and X.-H. Li, Schottky Barrier-Induced Surface Electric Field Boosts Universal Reduction of  $\text{NO}_x^-$  in Water to Ammonia, *Angew. Chem. Int. Ed.*, 2021, **60**, 20711-20716.
6. A. Ozden, Y. Wang, F. Li, M. Luo, J. Sisler, A. Thevenon, A. Rosas-Hernández, T. Burdyny, Y. Lum, H. Yadegari, T. Agapie, J. C. Peters, E. H. Sargent and D. Sinton, Cascade  $\text{CO}_2$  electroreduction enables efficient carbonate-free production of ethylene, *Joule*, 2021, **5**, 706-719.
7. Y. Han, X. Zhang, W. Cai, H. Zhao, Y. Zhang, Y. Sun, Z. Hu, S. Li, J. Lai and L. Wang, Facet-controlled palladium nanocrystalline for enhanced nitrate

- reduction towards ammonia, *J. Colloid Interface Sci.*, 2021, **600**, 620-628.
8. J. Li, G. Zhan, J. Yang, F. Quan, C. Mao, Y. Liu, B. Wang, F. Lei, L. Li, A. W. M. Chan, L. Xu, Y. Shi, Y. Du, W. Hao, P. K. Wong, J. Wang, S.-X. Dou, L. Zhang and J. C. Yu, Efficient Ammonia Electrosynthesis from Nitrate on Strained Ruthenium Nanoclusters, *J. Am. Chem. Soc.*, 2020, **142**, 7036-7046.
  9. Y. Wang, A. Xu, Z. Wang, L. Huang, J. Li, F. Li, J. Wicks, M. Luo, D.-H. Nam, C.-S. Tan, Y. Ding, J. Wu, Y. Lum, C.-T. Dinh, D. Sinton, G. Zheng and E. H. Sargent, Enhanced Nitrate-to-Ammonia Activity on Copper–Nickel Alloys via Tuning of Intermediate Adsorption, *J. Am. Chem. Soc.*, 2020, **142**, 5702-5708.
  10. H. Liu, X. Lang, C. Zhu, J. Timoshenko, M. Rüscher, L. Bai, N. Guijarro, H. Yin, Y. Peng, J. Li, Z. Liu, W. Wang, B. R. Cuenya and J. Luo, Efficient Electrochemical Nitrate Reduction to Ammonia with Copper-Supported Rhodium Cluster and Single-Atom Catalysts, *Angew. Chem. Int. Ed.*, 2022, **61**, e202202556.
  11. X. Zhang, Y. Zhang, P. Shi, Z. Bi, Z. Shan and L. Ren, The deep challenge of nitrate pollution in river water of China, *Sci. Total Environ.*, 2021, **770**, 144674.